Biomedical Signal Processing and Control 86 (2023) 105237

Contents lists available at ScienceDirect

Biomedical Signal Processing and Control

journal homepage: www.elsevier.com/locate/bspc

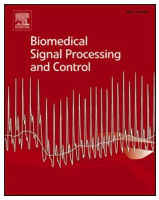

Advanced framework for enhancing ultrasound images through an optimized hybrid search algorithm and a novel motion compounding processing chain

Ahmed F. Elnokrashy [a,b,*], Laila N. Abdelaziz [a,*], Ashraf Shawky [a], Radwa M. Tawfeek [a]

[a] Electrical Engineering Department, Benha Faculty of Engineering, Benha University, Benha, Egypt
[b] Computer Science Department, Faculty of Information Technology and Computer Science, Nile University, Giza 12677, Egypt

ARTICLE INFO

Keywords:
Speckle noise
Motion compounding
O-MTSS
Image evaluation metrics
Ultrasound image

ABSTRACT

Ultrasound imaging is a fast, widespread, and essential diagnostic technique for examining the body's internal anatomy to find abnormal tissues or diseases. However, speckle noise in ultrasound imaging corrupts fine details and edges and degrades the image's resolution and contrast, making diagnosing more difficult. In this work, a speckle reduction method using motion compounding is proposed. The objective of this work is ultrasound image enhancement keeping all the diagnostics details and edges. The proposed method uses the pre-locations frames that the sonographer generates before locating the required diagnostic frame. These frames are applied to the proposed optimized Modified Three-Step Search (O-MTSS) algorithm to enhance the final processed frame. The O-MTSS algorithm is a hybrid between the Three Step Search algorithm (TSS) and the New Diamond Search Algorithm (NDS). The method requires a scoring layer for storing additional frames to select optimal frames that will be used for enhancement. The proposed methodology is tested on synthetic and real ultrasound images. The outcomes produce considerable speckle reduction while maintaining the image edges with good computational time for real-time scanning. The result is evaluated by subjective physicians, radiologists, and image evaluation metrics. According to the percentages of the subjective analysis, there is a remarkable improvement in the processed image. The proposed algorithm result is compared with existing algorithms; It is observed that the improvement in terms of signal to noise ratio, peak signal to noise ratio, mean square error, root mean square error and structural similarity index values of the proposed method are 4.6%, 3.32%, 12.02%, 6.2% and 1.57% respectively over Non-Local Low-Rank (NLLR) method. According to qualitative and quantitative analysis, the suggested method outperforms existing speckle reduction techniques regarding edge and fine detail preservation.

1. Introduction

Ultrasound imaging is becoming more popular in clinical diagnosis and is preferred for many reasons. It has many advantages compared to computed tomography (CT) and magnetic resonance imaging (MRI), such as being low-cost, portable, non-invasiveness, more economical, harmlessness, and compact while being free from ionizing radiation and offers real-time operation [1–3]. Ultrasound scanners obtain ultrasound images (USI) according to the principle of ultrasonography (echo imaging). The pulsed sound waves generated by the scanner are applied to the body's tissues [2,4]. Unfortunately, UIs contain speckle noise due to the destructive or constructive interference between different ultrasonic waves during the image generation phase [5–7]. Speckle noise is an unfavourable factor in USI because it complicates the diagnosis of diseases by clinicians. In order to perform better analyses and diagnoses in many applications (such as object detection and visualization of body organs), reducing noise in US medical images is a crucial step that has evolved into a preprocessing requirement. This is done without affecting crucial diagnostic features in the image [7]. Several methods have been developed to solve this problem [6,8].

Inspired by the early researchers' works in speckle noise reduction to improve the quality of US medical images while maintaining the fine details, this paper proposes a method using MC with optimized modified three-step search (O-MTSS) for the despeckling of USI. The modified three-step-search (MTSS) is used in the proposed method, one block matching algorithm suitable for video compression for computing

* Corresponding authors at: Electrical Engineering Department, Benha Faculty of Engineering, Benha University, Benha, Egypt (A.F. Elnokrashy).
E-mail addresses: ahmed.elnokrashy@bhit.bu.edu.eg (A.F. Elnokrashy), lyla.naser@bhit.bu.edu.eg (L.N. Abdelaziz).

https://doi.org/10.1016/j.bspc.2023.105237
Received 2 April 2023; Received in revised form 13 June 2023; Accepted 3 July 2023

motion vectors (MV) between two frames.

The proposed method is implemented and applied on synthetic USI by field II simulation software and real USI. Subjective radiologists, physicians, and objective quantitative criteria evaluated the reconstructed images. The results are compared with well-known despeckling algorithms to prove the suggestion's merit. For comparison and performance evaluation, quality evaluation metrics, including SNR, root mean square error (RMSE), peak signal to noise ratio (PSNR), mean square error (MSE), structural similarity index (SSIM), an equivalent number of looks (ENL) and calculation time are considered.

The main contributions of this work are:

- To the best of our knowledge, it is the first time to propose a practical and implementable processing chain for ultrasound image enhancement using motion computing. There are no extra steps for regular scanning without any overheads added to the scanning.
- A hybrid search algorithm, which utilizes the three-step search (TSS) and the newly developed diamond search (NDS) algorithms, has been proposed for motion compensation to find MV macroblocks between the old and current frames.
- Due to the computationally intensive nature of motion detection techniques, an optimized implementation framework is proposed to enable algorithm implementation on contemporary PC systems.

The rest of this paper is structured as follows: The background of the modified three-step search technique and the new cross-hexagonal search algorithm are shown in Section 2. Section 3 presents the suggested methodology in detail. Results and discussions using synthetic and actual data are presented in Section 4. Finally, Section 5 concludes the work.

2. Related work

Speckle noise can be improved using various techniques, including compound imaging or frame-based processing. Frame-based processing can be done using the spatial domain, transform domain, and deep learning. In contrast, image compounding can be done by frequency compounding (FC), spatial compounding (SC), and motion compounding (MC) [9].

The transform domain technique alters the transform coefficients, whereas spatial domain techniques operate directly on the pixels [10]. All methods of compounding images are created by generating multiple images of the speckle noise distribution that is pertinent. These images are then statistically averaged. This can be achieved by either changing the angle of the ultrasound beam in the SC or varying the imaging frequency between different frames in the FC. The MC technique combines many successive frames when the probe moves or when there is an involuntary movement, such as a heartbeat or stomach movement. Motion compensation of the frames prior to averaging is necessary because direct frame averaging could result in blurring and losing the boundaries of the organs [9].

Although the frame-based processing does not decrease the frame rate, information losses must occur due to the lower signal to noise ratio (SNR). Although with a lower frame rate, the methodology based on compound imaging is still essential for image enhancement because it can improve the image's texture without losing too much detail [9].

Some of the popular US speckle noise reduction techniques are Lee [11] and Kuan [12] filters which are based on reducing the Mean square Error; the Frost filter uses an exponential damped kernel to maintain the slight edges [13]. In addition, the Median filter is best for removing impulsive noise from images [14], and the Mean filter is simple, and the most efficient noise reduction filter; however, a blurred effect is produced [15]. Bilateral filter [16] and Anisotropic diffusion [17] are the most effective techniques due to their excellent edge preservation ability. However, these techniques do poorly with images of significant noise because they distort the correlations between neighbouring pixels [18,19]. Tay et al. created a squeeze box filter (SBF) to eliminate speckle noise, which was motivated by the concept of reducing pixel fluctuation in homogeneous regions while retaining (or enhancing) the variations in the mean values of various regions [20].

Zhu et al. [21] introduced a low-rank non-local filter that utilized a guiding image to help choose possible patches for non-local filtering when there were large speckles. Non-local methods always search for comparable patches within a square window. This technique does not, however, always work well for edge areas. The patch size must also be pre-learned before being fixed for the test images. Considering the superpixel characteristics around the region's edges, Chen et al. [5] presented a superpixel version of binary filtering to protect the local structure better while removing noise.

Mei et al. [22] presented a technique that consists of three steps. The first step is estimating the noise-free image using an enhanced Optimal Bayesian Non-Local Means (OBNLM) filter, where a new vector form represents each pixel patch. In the second step, the parts of the picture with low redundancy are then identified using a new index termed the redundancy index of each pixel patch. Finally, to recalculate the filter output and construct the suggested approach's final result, another new vector form is employed to represent the pixel patch in low redundancy areas acquired in the next step. This technique has high complexity, and Low contrast features are typically severely blurred.

Zhang et al. [23] presented a novel hybrid method in which Nonlinear Coherence Diffusion (NCD) and Laplacian Pyramid Based Nonlinear Coherence Diffusion (LPNCD) are combined. The novel method shows a strong capacity to maintain tissue features while improving coherence. Shereena et al. [10] introduced a novel non-local means (NLM)-based model in which the input picture is subjected to Grey Wolf Optimization (GWO) in order to obtain the design parameters of the NLM filter. The NLM filter receives the optimal parameters and the noisy picture to produce the denoised image. Salih et al. [24] presented a novel noise reduction scheme for USI by implementing the kernel principal component analysis (PCA) into the NLM and computing the similarity in a high-dimension kernel PCA subspace. The kernel representation can perform better even in highly noisy conditions since it resists noise. Additionally, it considers the pixels' higher-order statistics, which can result in perfect edge preservation.

In the transform domain techniques, the most widespread transformation is the wavelet transform used for converting from the time domain to the frequency domain, and the inverse wavelet transform is used in reverse. Nowadays, wavelet transform is used for removing speckles from USI [25]. Some of these techniques, multiscale transformations like contourlet, Ridgelet, and wavelet, have been suggested by Nisha et al. [26]. Coefficients are thresholded using Sureshrink, Bayeshrink, and Neighsureshrink after decomposition. Different MRI and CT images are used. According to SSIM, PSNR, and WSNR metrics, Neighsureshrink with Contourlet-based denoising produced higher results for medical images.

Sirapat Chiewchanwattana et al. [27] introduced a despeckling filter intending to maintain all necessary properties without degradation. The suggested technique uses a cuckoo search algorithm and an adaptive thresholding function (CS-WT thresholding adaptive filter). With less complexity, lower MSE, and MAE, it keeps the textures, edges, and lines. Comparatively, PSNR and SSIM are better than other optimization techniques. Leena Jain et al. [28] suggested a new, more general thresholding function for speckle reduction that was utilized in conjunction with the Daubechies 8 wavelet as the decomposition function with two levels. Saurabh Khar [29] presented a method that used a non-local means (NLM) filter with square-chord distance to reduce speckle noise from the DWT approximation coefficients and low rank-based Weighted Nuclear Norm Minimization (WNNM) in order to reveal the sparsity property of DWT.

Simone Cammarasana et al. [30] developed a new deep-learning architecture for the real-time noise removal of ultrasound pictures. First, state-of-the-art methods are compared for denoising (such as low-

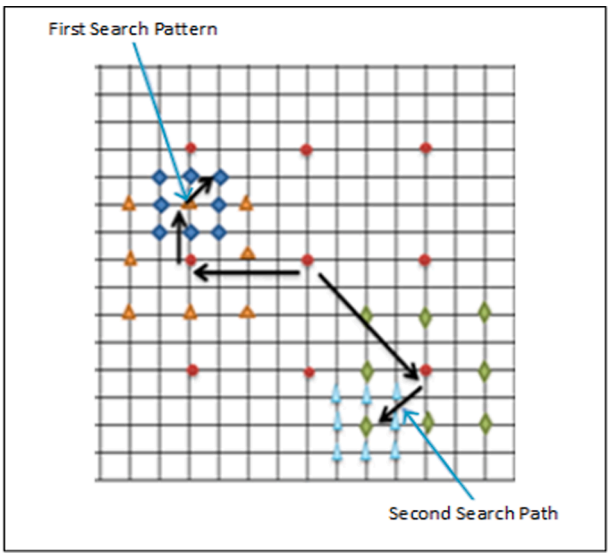

Fig. 1. Two different search paths for TSS.

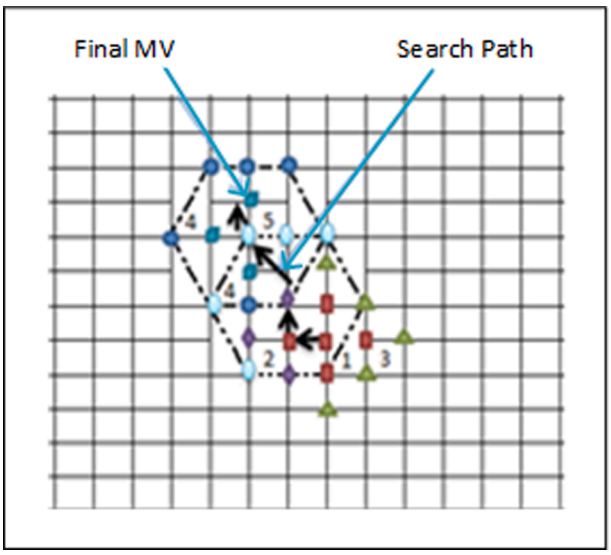

Fig. 2. Search path in New Hexagon Search motion estimation.

rank and spectral approaches) and determined that WNNM (Weighted Nuclear Norm Minimization) provided the highest accuracy, retention of anatomical details, and edge enhancement. After that, they suggested a tuned variation of WNNM (tuned-WNNM), which increased the quality of the denoised pictures and expanded its application to USI. Using a deep learning architecture, the tuned WNNM duplicated WNNM findings in real-time, both qualitatively and numerically. Kai Zhang et al. [31] used the construction of feed-forward denoising convolutional neural networks (DnCNNs) for image denoising, independently from the noise level.

Ahmed F. Elnokrashy [9] presented an MC method based on O-ARPS for motion estimation in the compounding technique. When the US probe or the scanned organ is slightly moved, the speckle pattern will become decorrelated. The tissue will be distorted, and the picture will be blurry when the USI is directly compounded. So, prior to compounding, motion estimation (ME) is required. Experimental in vivo images demonstrated that the speckle noise was significantly decreased without degrading the boundary of the organ. Additionally, enhanced picture perception was accomplished by maintaining a few texture features with Timing Performance close to real-time.

3. Background

3.1. Three step search algorithm (TSS)

TSS, proposed by Koga et al. [32], is one of the efforts to perform a fast motion estimation algorithm. The first step in this algorithm is to define the search window (SW) size, search for the best matching, and plot 9 points in the centre of SW at an equal distance of step size (SS). Motion error measurement or block distortion measure (BDM) is usually used for block matching (BM) to calculate the difference between two blocks. There are two main error measurements, the sum of absolute difference (SAD) represented in Eq. (1) and the sum of squared errors (SSD) calculated by Eq. (2).

$$SAD = \sum_{y=1}^{MB_y} \sum_{x=1}^{MB_x} |I(x,y,t) - I'(x,y,t-1)| \quad (1)$$

$$SSD = \sum_{y=1}^{MB_y} \sum_{x=1}^{MB_x} [I(x,y,t) - I'(x,y,t-1)]^2 \quad (2)$$

where MB_y, MB_x are the row and column of the macroblock. x and y are the indexes of column and row, respectively. I and I' are the pixels' values compared to the current and previous macroblocks.

The TSS algorithm is summarized as follows:

1. Plot 9 points in the SW at a step size ss = 4 and check 9 points in the 9 × 9 SW.
2. The step size is divided by 2, i.e., ss = 2, and 8 points are checked to generate a 5 × 5 square shape pattern. If the minimum BDM is one of the 9 points, this point is considered a centre point in step 3.
3. Step size is divided by 2, i.e., ss = 1, and check 8 points to generate a 3 × 3 square shape pattern, and the search will be terminated.

The final MV is the minimum BDM point at the 3 × 3 square shape pattern. Fig. 1 shows the two different search paths of TSS for estimating an MV within the SW. TSS can be easily extended to an n-step search for a larger SW. Twenty-five points are required to check for TSS.

3.2. New cross hexagonal search algorithm (NCHEXS)

NCHEXS was proposed by Kamel Belloulata et al. [33]. In this algorithm, two small/large cross patterns (SCSP/LCSP) were used as the initial three steps and two small/large hexagonal patterns (SHSP/LHSP) as the later step of the search. Fig. 2 shows the search path of NCHEXS. At the beginning of this algorithm, initialize SCSP by plotting 5 points at the centre of SW. The algorithm is summarized as follows:

1. Stop searching if the SCSP's centre contains the smallest BDM point; otherwise, move on to step 2.
2. Stop searching if the minimum BDM point is at the centre of a newly formed SCSP; otherwise, move on to step 3.
3. Check two unchecked points of the square centre biased and three unchecked points of the LCSP to show the best possible hexagonal search direction.
4. A new LHSP is formed by considering a centre point as the minimum BDM point in the previous step. If the minimum BDM point is found at the centre of a new LHSP, go to step 5; otherwise, again form a new LHSP, i.e., repeat step 4.
5. If the minimum point is found at the centre of the LHSP, shift to the SHSP and find the best MV.

3.3. Modified three step search algorithm

MTSS, proposed by Kamble et al. [34], is one of the search algorithms to perform a fast motion estimation algorithm. The MTSS combines two

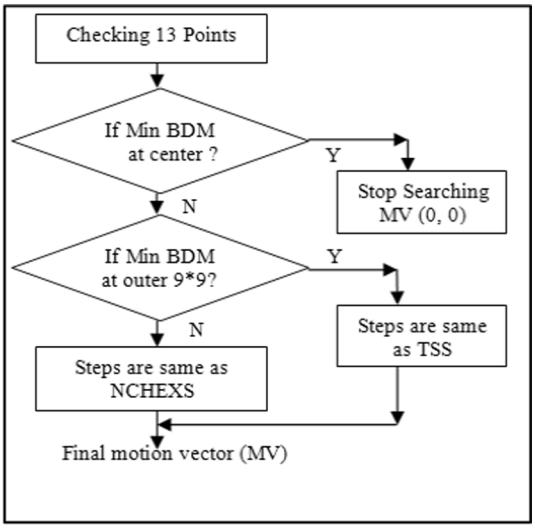

Fig. 3. Flowchart of MTSS.

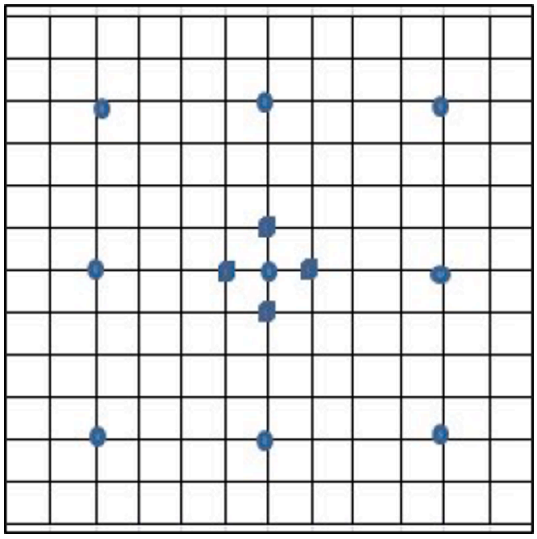

Fig. 4. The first step in MTSS.

approaches: TSS and NCHEXS. The MTSS approach estimates an MV compared to the previous frame.

Fig. 3 shows the flowchart of MTSS and has the following steps:

1. Initially, MTSS started using the first step from TSS and NCHEXS, so 13 points are checked, as shown in Fig. 4.
2. TSS will execute if the minimum BDM point is found at the outer point of the 9 × 9 SW.
3. If the minimum BDM point is found at the four outer points of the SCSP, then NCHEXS will execute.

The two search paths of the proposed MTSS approach are shown in Fig. 5.

4. Methodology

In MTSS, the first step in TSS and the NCHEXS are checked, and since the motion measure error (ME) is the least, the search continues on its path, as shown in Fig. 4. However, this method is not always correct in finding MVs because the first step may be wrong and, therefore, will continue on the wrong path. As a result, the MTSS is modified to

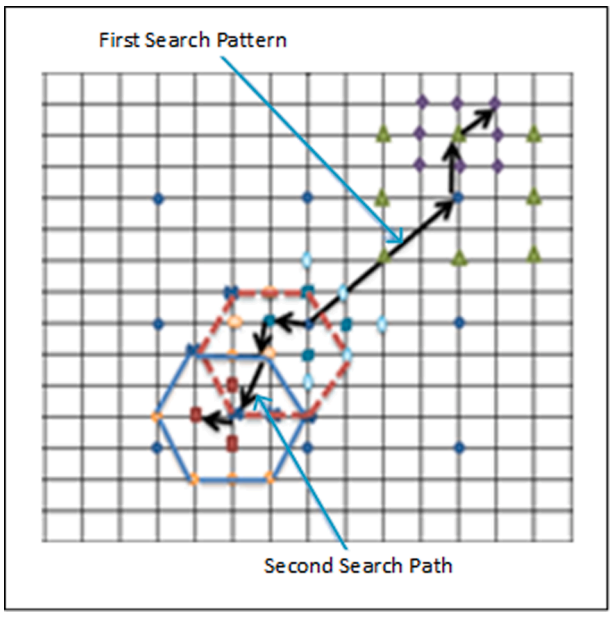

Fig. 5. Two search paths in MTSS.

continue in the path that achieves two minimum consecutive ME, and the NCHEXS is replaced with a new diamond search (NDS) specifically designed to address the ultrasound images.

This paper proposes a complete workflow to implement a despeckling ultrasound image framework. The proposed method passes through four stages, as shown in Fig. 6. First, the preprocessing stage uses a filter to remove the white noise and enhance motion detection. Second is the motion detection stage, in which the motion is detected by calculating the MV between the different frames. Third, the frame selection stage, in which each frame is chosen to be stored or omitted.

Finally, the compensation stage averages the compensated frames and reduces the speckle noise. These stages are explained in detail in the following subsections.

4.1. Preprocessing

At this stage, a preprocessing step is performed on the ultrasound images (frames) before applying the O-MTSS algorithm. Specifically, a low-pass filter in the form of a Gaussian filter is applied to remove the white Gaussian noise that is inherent in the hardware of the ultrasound machine. This filter also serves to enhance motion detection. The search for the correct MV may fail if the macroblocks lack correlation. Although the correct MV may be close, the search algorithm may fail to find it. However, applying a low-pass filter enables better correlation between the adjacent blocks, thereby improving the accuracy of the MV's absolute error result., as shown in Fig. 7.

4.2. Motion detection

Estimating motion in ultrasound is challenging due to the nature of spots associated with ultrasound frames. Several block-matching algorithms have been proposed to estimate motion displacement in ultrasound frames [9]. This paper proposes the O-MTSS, a block-matching algorithm, to enhance the compound motion image. O-MTSS is an optimized version of the original MTSS.

The proposed O-MTSS approach calculates motion compensation prediction error (MCPE) between two successive frames. The O-MTSS approach is a hybrid algorithm that combines the New Diamond Search algorithm (NDS) and TSS algorithm. The NDS algorithm employs one search pattern, as shown in Fig. 8. In the NDS, the pattern will repeat itself until the minimum BDM point is the pattern's centre or the search

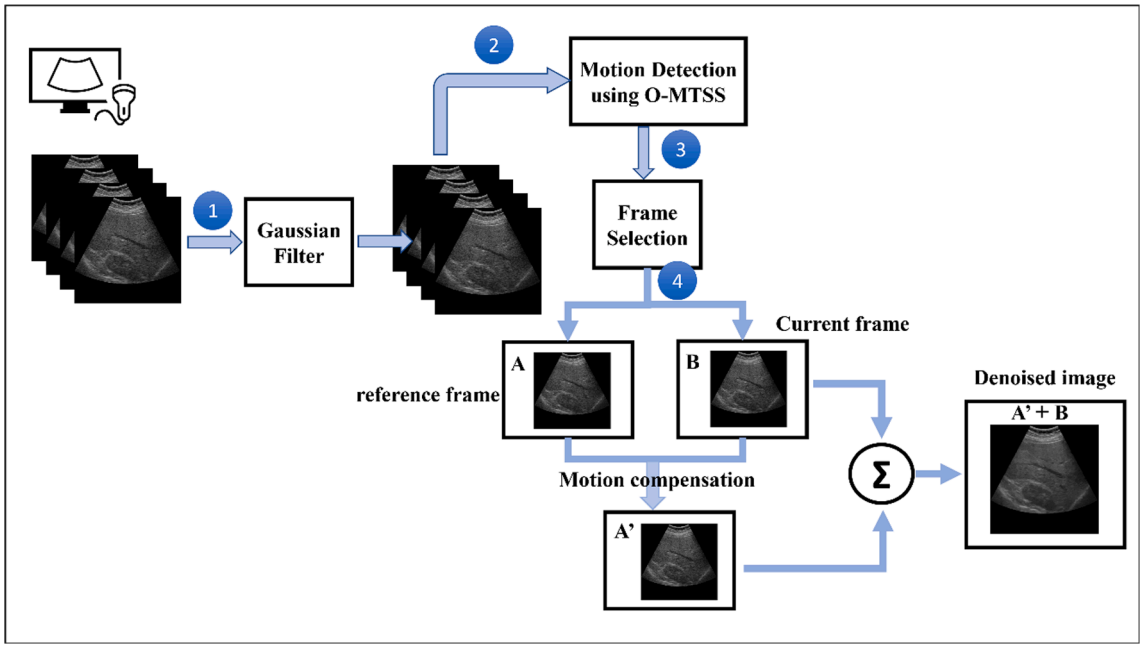

Fig. 6. The procedure of the proposed method.

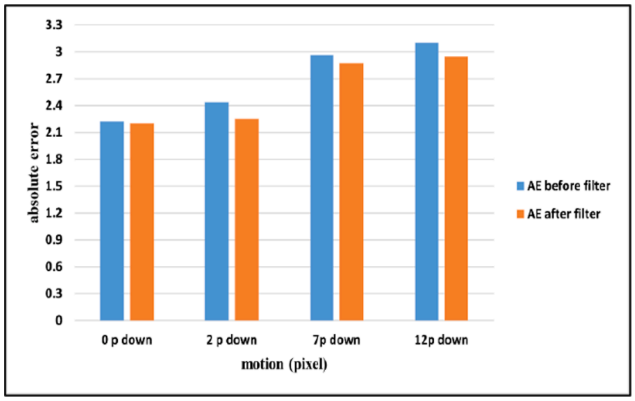

Fig. 7. The effect of the Gaussian filter on absolute error.

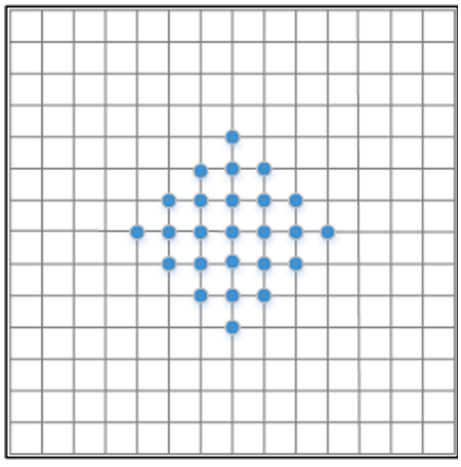

Fig. 8. New Diamond Search (NDS) pattern.

is outside the search window.

In the O-MTSS algorithm, a decision is taken for each MB whether to follow the search path of the NDS or the TSS. This decision is based on which path will achieve two minimum consecutive. In other words, a step is taken in both TSS and NDS to find the least minimum of the two searches. Then another step is taken in both paths and finds the least minimum. If TSS gets two consecutive minimums, the search continues on this path and the same for NDS. The flowchart and two path searches for the proposed O-MTSS approach are illustrated in Figs. 9, 10, respectively.

The O-MTSS is summarized as follows:

1. One step in TSS is checked. If minimum BDM is found at the centre, then MV is zero and stop searching; otherwise, go to step 2.
2. One step in NDS is checked. Find the NDS minimum point.
3. If (TSS min < NDS min), increment the TSS counter and put zero to the NDS counter; else, increment the NDS counter and put zero in the TSS counter.
4. If the TSS counter equals two, continue in the TSS path illustrated in Fig. 1; otherwise, go to step 5.
5. If the NDS counter equals two, continue in the abovementioned NDS path; otherwise, go to step 1.
6. If the TSS is outside the search window, continue in the NDS path and compare the minimum of them; otherwise, go to step 8.
7. If (TSS min < NDS) min, then TSS point in the final mv; otherwise, NDS point is the final MV.
8. If the NDS is outside the search window, continue in the TSS path, compare the minimum, and go to step 7.

4.3. Frame selection

The motion compounding approach depends on compounding different decorrelated speckle noise frames. If there is no significant movement between the frames, compounding these frames will not be enhanced. So, the frames that will be used must be selected according to a specific motion threshold. The threshold is selected experimentally based on the try-and-error method to find the suitable threshold.

The sum of the absolute of all MVs of the frame is calculated. Three cases are rested against the chosen threshold. First, when the motion between frames is close to the threshold, there is a motion between the

```
Input : Current frame; Reference frame; SW
Output : MV
Begin
TSS costs(2,2) = calculte TSS cost at the centre
If TSS costs(2,2) ≃ 0 Then
    MV = (0,0)
    Else
        While TSS & NDS inside the SW Do
            call TSS
            If minTSS ≃ 0 Then
                MV = this point
                Else
                    call NDS
                    If minNDS ≃ 0 Then
                        MV = this point
                        Else
                            if minTSS < minNDS Then
                                TSScount + = 1
                                NDScount =0
                                Else
                                    NDScount + = 1
                                    TSScount = 0
                            Endif
                            If TSScount == 2 Then
                                continue in TSS path
                                MV = TSS point
                                Elseif NDScount == 2 Then
                                    continue in NDS path
                                    MV = NDS point
                            Endif
                    Endif
            Endif
        Endwhile
        If TSS out from sw Then
            continue in NDS path and find minNDS
            If minTSS < minNDS Then
                MV = TSS point
                Else
                MV = NDS point
            Endif
            Else
                continue in TSS path and find minTSS
                If minNDS < minTSS Then
                    MV = NDS point
                    Else
                        MV = TSS point
                    Endif
        Endif
Endif
End
```

Fig. 9. Pseudo code of motion detection using O-MTSS.

frames in the same body area, and these frames are stored for motion compounding. Second, when the motion between frames is less than the threshold, there is almost no motion, and the frame is neglected. Finally, when the motion exceeds the upper threshold, this indicates a significant motion. In this case, the frame buffer is reset, and the current frame is considered the first frame of the new location.

4.4. Compensation and average

4.4.1. Motion detection optimization

At first, the MBs always start their search from zero (the Centre point). The body's organs always move together. Hence, starting every time from the beginning to calculate the MV is not necessary.

During the search, the last two consecutive MVs are compared. If the average MV is taken, the value of the following MV can be expected. So, the search will start from the average MV point of the previous MBs. The average can be in the second order (i.e., take the average of two MV

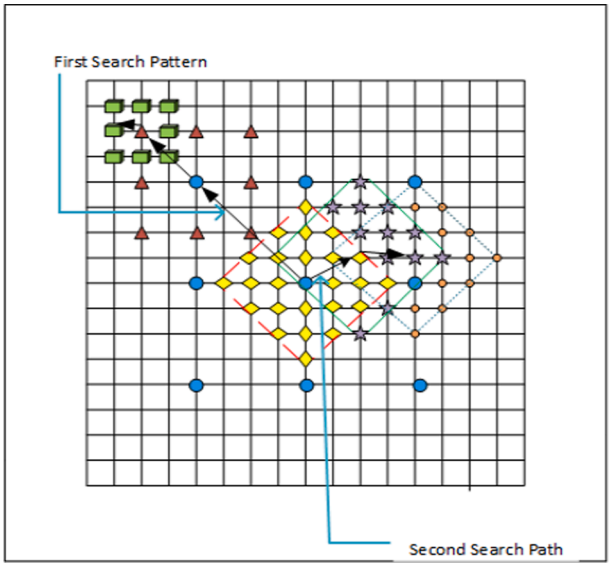

Fig. 10. Two search paths in O-MTSS.

Table 1
Evaluation Parameters.

	Definition	Equation
SNR	The amount of image noise content [35]. The higher the ratio, the better the image quality	$SNR = \frac{I_f(i,j)}{\sqrt{MSE}}$
PSNR	PSNR measures the similarity of the image Ir with the image If [35 36], and It is usually represented in decibels (dB) [37].	$PSNR = 10\log_{10}\frac{L^2}{MSE}$ Where, L: the largest possible value of the intensity in the original image.
MSE	MSE is a distortion measure [37]. The lower value of the MSE shows a minimal error [35].	$MSE = \frac{\sum_{(i,j)}^{R,S}[I_f(i,j) - I_r(i,j)]^2}{R \times S}$
RMSE	RMSE indicates the nearness between two images: the lower value, the better-quality image [35].	$RMSE = \sqrt{MSE}$
SSIM	SSIM compares two separate images' contrast, structure, and luminance [38]. The range of SSIM values is [-1, 1]	$SSIM = \frac{(2\mu_r\mu_f + c_2)(2\sigma_{rf} + c_2)}{(\mu_r{}^2 + \mu_f{}^2 + c_1)(\sigma_r{}^2 + \sigma_f{}^2 + c_2)}$ Where, μ_r, μ_f: the local means. σ_r, σ_f: standard deviations. σ_{rf}: cross-covariance for images. C_1 and C_2 are constants to avoid instability.
ENL	ENL measures the speckle noise level in a denoised image's homogeneous area [39]. A higher value of ENL shows effective suppression of speckles [40].	$ENL = \frac{mean^2(f)}{variance^2(f)}$

before), third order (average three MV before), and so on. When using average MV, the search starts from a known place, and there is a high probability that it will be close to the solution. This will significantly speed up finding the MV, reducing time and error.

Finally, the computed MV is used for each block to compensate for the movement in the new frame, and then a statistical average of the compensated frames is taken to reduce the speckle noise. According to the US sonographer, this can be done using more frames if higher

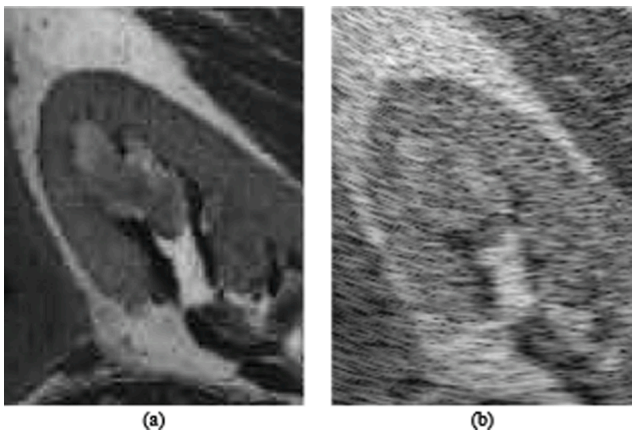

Fig. 11. Simulated speckle noise. (a) Reference MRI image for the comparison. (b) Noisy Field II image.

smoothness is required.

Fig. 6, step 4, shows the processing stages for motion compensation and compounding, in which a preprocessing filter is applied to the old and current frames, motion compensation is made between them, and the compensated frame is statistically averaged.

4.4.2. Image evaluation parameters (IEP)

Image Evaluation Parameters (IEP) are essential in measuring a processed image's performance or quality. Here, six sorts of IEPs, such as Signal Noise Ratio (SNR), Peak Signal to Noise Ratio (PSNR), Mean Square Error (MSE), Root Mean Square Error (RMSE), Structural Similarity Index Measure (SSIM), and Equivalent Number of Looks (ENL), are used in this work. A technique that requires an original image free of noise is known as a full reference metric, while metrics that use only the image without noise and a noisy image are non-referenced. Here, I_r denotes the reference or noise-free image, I_f is the filtered or denoised image and I_n represents the noisy image. R and S indicate the size of the image. The term (i, j) is used to represent the spatial position of a pixel. Table 1 illustrates a summary of the used parameter along with their definition.

5. Results

This study evaluated and compared the performance of a proposed methodology for despeckling ultrasound images (USI) to other well-known despeckle algorithms. To validate the effectiveness of the proposed method, synthetic and simulated USI obtained using Field II Simulation software and real USI were used and compared with the other methods. The comparison results demonstrated the proposed methodology's effectiveness in reducing speckle noise in USI.

Table 3
The ENL metric for different methods on kidney images depends on each region of interest (ROI).

Methods	ROI (red)	ROI (blue)	ROI (magenta)
Noisy image	0.0355	0.0428	0.055
Lee	5.0887	6.5087	**2.6679**
SRAD	3.4453	3.0170	2.1417
DnCNN	0.9345	1.9166	0.6403
O-ARPS	0.4187	0.3493	0.5254
NLLR	**5.7492**	2.9575	0.7693
Proposed method	3.8792	**8.9247**	1.3221

5.1. Results on synthetic simulated US

The Field II Toolbox simulates ultrasound scanner images [5,41]. The synthesized image looks very close to the real ultrasound image, as shown in Fig. 11. Reference images (with low noise level or without noise) are used to compare the denoising output to determine the improvement in image quality and evaluate the methodology's effectiveness. Usually, reference and noisy images can be obtained using the same scanner and operating conditions. This is very difficult due to the high dependence on the operator for ultrasound exams and the random variation of speckle phenomena in each acquisition and scattering [42]. In this case, traditional quality metrics cannot indicate the quality obtained by speckle reduction. So, it is helpful to use synthetic images obtained, for example, by computer simulations or anatomical phantoms. In our study, Field II is used to simulate a B-mode ultrasound image Fig. 11(b) from a noise-free MRI of a kidney as the reference image for speckle reduction evaluation Fig. 11(a).

In this research, an 8-bit grey-level kidney standard image (148 × 196 pixels) is used to evaluate the effectiveness of noise reduction Fig. 11(a). The speckle noise is added to the image by Field II. All image processing was performed with MATLAB® (R2021a MathWorks). The used system configuration consists of a personal computer with a 3rd generation Intel® Core™ i7-3610QM running at 2.30 GHz and using 64-bit Windows 10 Pro with 8 GB of RAM.

The proposed method is compared with four techniques, local statistics-based filtering (Lee) [11,43], the speckle reducing anisotropic diffusion (SRAD) [17,44], the Denoising Convolutional Neural Networks (DnCNNs) [31], the Optimized Adaptive Rood Pattern Search (O-ARPS) [9] and the Non-Local Low-Rank method (NLLR) [21]. The proposed method used four frames with different speckle patterns for averaging and a 16 × 16 macroblock size.

Table 2 and Table 3 summarize the performance of the speckle reduction techniques applied to the simulated Field II kidney image by calculating several performance metrics. Table 2 reveals that the proposed method is better than all other speckle reduction methods in SNR, PSNR, MSE, RMSE, SSIM and some ENL values among the four speckle noise reduction methods in the kidney image. SNR improvements of the proposed O-MTSS method over that of the NNLR and O-ARPS methods are 4.6% and 8.58%, respectively. PSNR improvements of the proposed

Table 2
Image quality metrics for different methods on kidney image.

Methods	SNR	PSNR	MSE	RMSE	SSIM	Time (sec)
Noisy	9.167	13.523	2888.947	53.7489	0.12562	–
Lee	9.942	14.435	2341.981	48.394	0.38817	0.5093
SRAD	9.82	14.269	2433.215	49.3276	0.37126	**0.506**
DnCNN	10.99	16.234	1547.786	39.3419	0.32449	–
O-ARPS	11.31	16.281	1530.953	39.1274	0.30669	2.196
NLLR	11.74	16.732	1380.066	37.1493	0.4589	1.627×10^3
Proposed method	**12.28**	**17.288**	**1214.146**	**34.8446**	**0.46609**	1.915

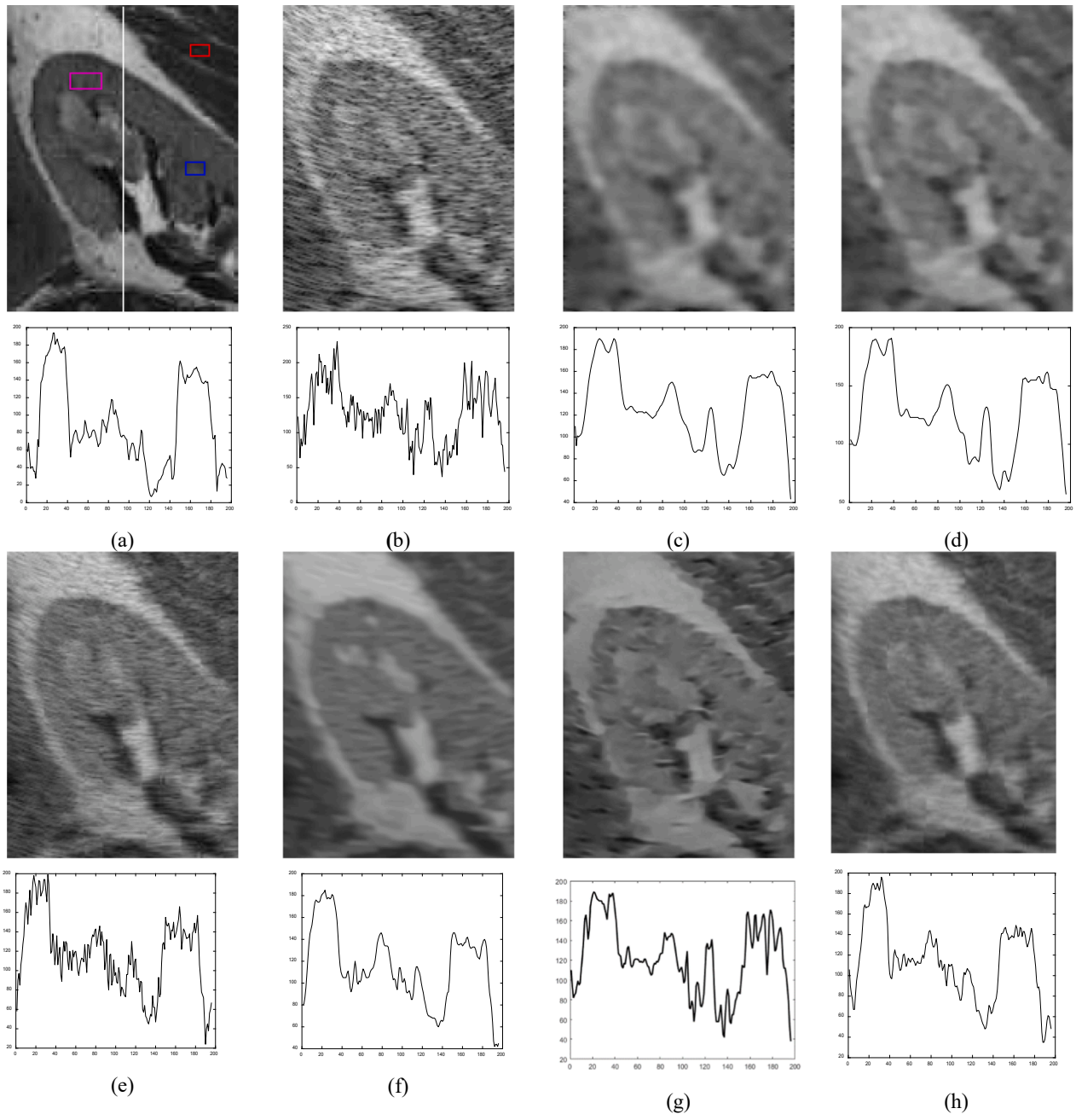

Fig. 12. Comparison of despeckling results on kidney Field II images with profiles. (a) Reference Image (b) Noisy "kidney" and the results by (c) Lee, (d) SRAD (e) O-ARPS, (f) NLLR, (g) DNCNN and (h) the proposed O-MTSS.

O-MTSS method over that of the NNLR and O-ARPS methods are 43.32% and 6.19%, respectively. MSE improvements of the proposed O-MTSS method over the NNLR and O-ARPS methods are 12.02% and 20.7%, respectively. RMSE improvements of the proposed O-MTSS method over the NNLR and O-ARPS methods are 6.2% and 10.95%, respectively. SSIM improvements of the proposed O-MTSS method over that of the NNLR and O-ARPS methods are 1.57% and 51.97%, respectively. Table 3 lists the ENL values acquired in three ROIs. According to Table 3, the proposed method attains the highest ENL values of ROI (blue). This means the resulting image has excellent speckle noise suppression ability in the homogenous regions. In the ROI (red) and ROI (magenta), the proposed method obtains the third highest ENL values after NLLR and Lee, respectively.

It can be observed from Fig. 12 that our proposed method yields more satisfactory results in terms of visual performance. For Lee and SRAD, the denoised image in Fig. 12(c) and 12(d) are blurred. Based on Fig. 12(e), it is evident that the O-ARPS technique preserves the edges' boundary, but the speckle noise level remains significantly high. Fig. 12 (f) shows that the NLLR approach exhibits extended computation time, superior quality metric performance, and minimal image blurring. However, in some cases, a lower level of speckle noise could aid in diagnosis. The DNCNN illustrated in Fig. 12(g) effectively preserves edges and contrast; however, it struggles to accurately represent the original texture, especially in certain textures like the white band area and mid-range level kidney tissue. The denoised image by the proposed method in Fig. 12(h) shows an image with higher speckle noise reduction and edge preservation performance, and the image's details are well preserved. The profile of each image is obtained from a column in white on the noise-free (reference) image.

For a fair comparison, the suggested approach performance ratio of

Table 4
performance ratio of PSNR and SSIM for four denoising methods.

Methods	Method [28]	Method [29]	Proposed method
PSNR	3.6082%	6.9848%	**27.8415%**
SSIM	46.2258%	242.6667%	**271.0317%**

PSNR and SSIM is compared with the Leena Jain method [28] and Saurabh Khar method [29]. Table 4 reveals that according to the noisy image, the proposed O-MTSS has achieved the best performance ratio in both PSNR (27.8415%) and SSIM (271.031%). The performance ratio is calculated by the percentage of change equation in Eq. (3).

$$percentofchange = \frac{New - Original}{Original} \times 100 \tag{3}$$

Table 5
Doctors' scores for liver-kidney images.

Metrics	Evaluation score	Original	Img1	Img2	Img3	Img4	Img5
Smooth	**Score = 0**	6	0	0	0	0	0
	Score = 1	1	2	2	1	2	3
	Score = 2	0	3	3	4	1	0
	Score = 3	0	2	2	2	4	4
Contrast	**Score = 0**	5	2	1	1	1	1
	Score = 1	2	1	2	2	2	3
	Score = 2	0	2	3	3	3	2
	Score = 3	0	2	1	1	1	1
Diagnosis details	**Score = 0**	3	1	0	0	0	0
	Score = 1	4	2	2	2	3	2
	Score = 2	0	2	2	3	3	3
	Score = 3	0	2	3	2	1	2
Hidden details	**Score = 0**	1	3	3	1	0	0
	Score = 1	2	1	2	2	3	2
	Score = 2	2	2	2	4	4	5
	Score = 3	2	1	0	0	0	0
Clear boundaries	**Score = 0**	4	1	0	1	1	0
	Score = 1	3	1	0	0	1	2
	Score = 2	0	3	4	3	4	4
	Score = 3	0	2	3	3	1	1
Good image	**Score = 0**	5	2	1	1	1	1
	Score = 1	2	2	0	2	2	1
	Score = 2	0	3	4	2	4	4
	Score = 3	0	0	2	2	0	1

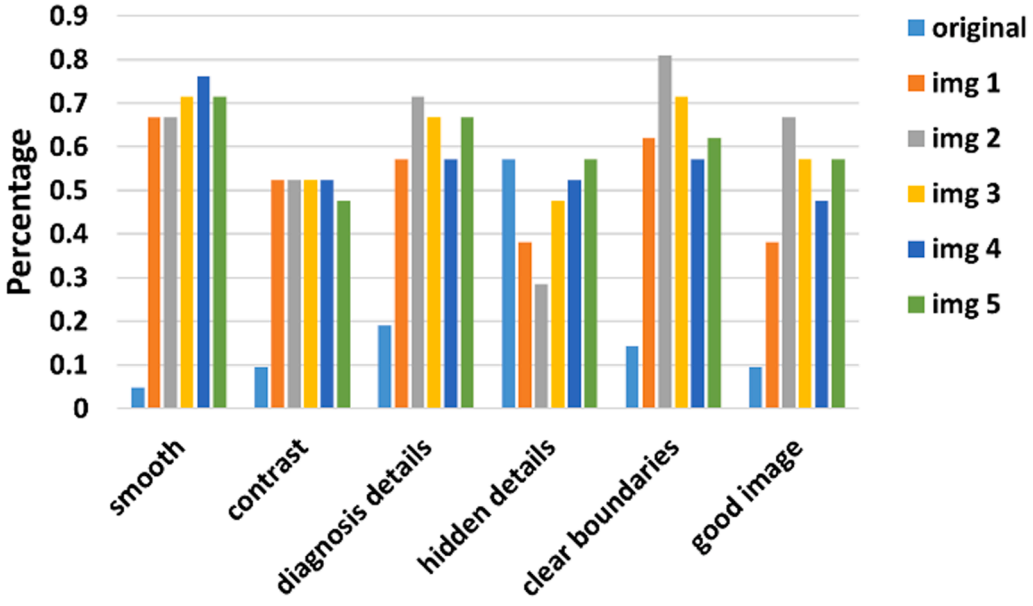

Fig. 13. Statistical analysis of the liver-kidney images.

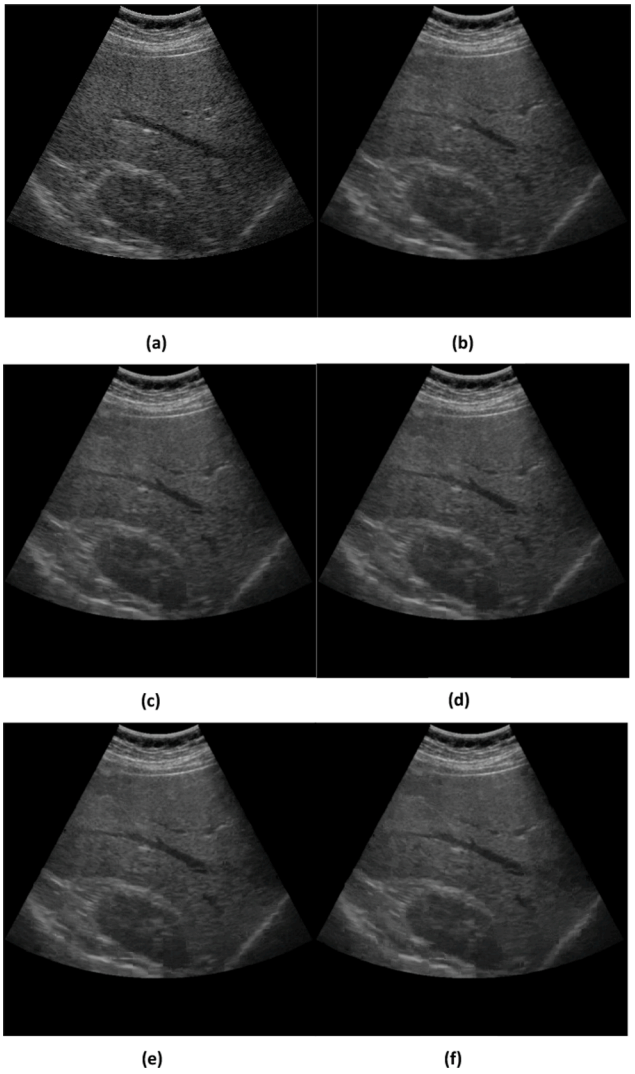

Fig. 14. Comparison of despeckling results on the liver-kidney image. (a) the original image and (b) the proposed method with frames 3,4,5,6 and 8, respectively.

5.2. Experiments on real USI

Although synthetic images can provide valuable insights, they may not encompass all the features in genuine ultrasound imaging conditions. Therefore, we also tested the proposed method on real ultrasound semi-videos of the liver and kidney captured using a Digisone IQ 32-channel US device. The proposed method's performance in terms of the diagnostic value of the obtained images was evaluated by seven physicians with expertise in radiology, hepatology, and gastroenterology, with experience levels ranging from 3 to 26 years. These physicians examined the images to determine their effectiveness in diagnosis.

Six images were created: the original image (the speckled noise image) and five enhanced images using the proposed method with different frame parameters. The six images were shuffled randomly, and their titles were neglected. The physicians ranked the images from 0 to 3 in terms of smoothing, contrast, diagnosis details, detecting the presence of hidden details, clear boundaries, and diagnostic quality, where 0 represented the lowest and three the highest level of performance for each evaluated property.

Table 5 illustrates the scores of seven physicians for all the images in Fig. 14 regarding some diagnostic metrics, while Fig. 13 compares the proposed method's performance in terms of statistics with those of the original image. The proposed method attained the highest grades for most of the statistics compared to the original image, as evident in Table 5 and Fig. 13. Based on subjective statistics analysis, image 2, with four frames, emerged as the best in all parameters except smoothing. In contrast, image 4 was the best, as indicated in Fig. 13.

Fig. 14 compares the result of real ultrasound images obtained from the proposed method with the original image, which shows the effect of the proposed approach on reducing speckle noise while keeping all the diagnostic details and edges. Table 6 illustrates the timing performance of the system under a different number of frames used for enhancement and with and without optimization.

Table 6
Time performance before and after optimization.

# Frames	Time performance (msec)			
	3	8	15	30
Before optimization	370	687	1674	2417
After optimization	63.33	69.35	85.41	99.720

6. Discussion

Ultrasound imaging is a widely used medical imaging technique that provides real-time images of internal organs and tissues. However, ultrasound images are often noisy and blurry, making it difficult for physicians to diagnose accurately. This study proposed a complete processing pipeline for ultrasound image enhancement to preserve all crucial details for better diagnosis.

The proposed pipeline uses previous frames and motion compounding for current frame enhancement. The effectiveness of the pipeline was evaluated by comparing it with other well-known despeckle algorithms using synthetic and real ultrasound images. Physician feedback, in addition to evaluation metrics, approved the quality of the proposed pipeline.

Motion compounding is a known technique; however, no previous research has explored its use in real cases. The proposed pipeline's motion compounding method guarantees high-quality images without losing important texture details and edges. Additionally, a new motion computing algorithm customized for ultrasound images was proposed.

Despite the pipeline's success, the timing performance needs further enhancement based on better hardware. The algorithms can also be further improved using previous frame motion detection data. It was also found that the assumption that physicians move the probe slightly until they find the required frame may not be valid in all cases, as some expert physicians can reach the required frame quickly. This can lead to the inability to find the required number of frames adequate for the enhancement.

In conclusion, the proposed processing pipeline significantly contributes to the field of ultrasound image enhancement. It uses motion compounding and a customized algorithm for ultrasound images to preserve important texture details and edges. The pipeline's quality was approved by physician feedback and evaluation metrics. However, the pipeline's timing performance needs further improvement, and the algorithms can be further improved using previous frame motion detection data.

7. Conclusion

This paper presented a new speckle reduction method based on motion compounding and proposed new method for motion detection called O-MTSS, which employs pre-located frames using MC to enhance the quality of the ultrasound denoising process with keeping all the diagnostics fine details and edges. The proposed method optimizes MTSS to improve motion detection and MV estimation by first employing Gaussian preprocessing filters on the frames. After that, the frame selection stage is used to choose the frames to be stored, followed by

compensation and average frames. The proposed method is evaluated using synthetic images, and its quality metrics are compared to other techniques. The results indicated that the proposed method outperformed other SNR, PSNR, MSE, RMSE, and SSIM techniques. The improvements in the proposed hybrid method's SNR, PSNR, MSE, RMSE and SSIM are 4.6%, 3.32%, 12.02%, 6.2% and 1.57%, respectively, over the NLLR method.

Moreover, the denoised image produced by the proposed method showed higher speckle noise reduction and edge preservation performance, and the image's details are well preserved. Furthermore, the proposed technique is evaluated using real USI through subjective radiologists and physicians, and the results showed image quality improvement compared to the original USI. Finally, further advancements in processing speed can be achieved by utilizing more advanced computing technologies such as GPUs or high-end CPUs.

The motion-compounding method has the potential for improvement through physician assistance and enhanced smoothing quality. Furthermore, we anticipate this method will exhibit more diagnostic features as the speckle noise is effectively removed. Therefore, further research should be conducted to explore its potential for enhancing diagnostic capabilities.

Furthermore, utilizing GPUs can provide ample processing capacity to pursue further enhancements. Previously, we faced certain limitations in maintaining real-time solutions and had to rely on mid-range GPUs.

Declaration of Competing Interest

The authors declare that they have no known competing financial interests or personal relationships that could have appeared to influence the work reported in this paper.

Data availability

Data will be made available on request.

References

[1] O. Karaoğlu, H.Ş. Bilge, İ. Uluer, Removal of speckle noises from ultrasound images using five different deep learning networks, Eng. Sci. Technol. an Int. J. 29 (2022), 101030, https://doi.org/10.1016/j.jestch.2021.06.010.

[2] K. Binaee, R.P.R. Hasanzadeh, An ultrasound image enhancement method using local gradient based fuzzy similarity, Biomed. Signal Process Control. 13 (2014) 89–101, https://doi.org/10.1016/j.bspc.2014.03.013.

[3] S. Kumar Pal, A. Bhardwaj, A.P. Shukla, S.K. Pal, A. Bhardwaj, A.P. Shukla, A review on despeckling filters in ultrasound images for speckle noise reduction, in: 2021 Int. Conf. Adv. Comput. Innov. Technol. Eng., 2021, pp. 973–978, https://doi.org/10.1109/ICACITE51222.2021.9404638.

[4] G. Rekha, B. Rupali, Liver ultrasound image enhancement using bilateral filter, Int. J. Eng. Tech. Res. 8 (2018) 2454–4698.

[5] Y. Chen, M. Zhang, H.M. Yan, Y.J. Li, K.F. Yang, A new ultrasound speckle reduction algorithm based on superpixel segmentation and detail compensation, Appl. Sci. 9 (2019) 1693, https://doi.org/10.3390/app9081693.

[6] S.H.C. Ortiz, T. Chiu, M.D. Fox, S.H. Contreras Ortiz, T. Chiu, M.D. Fox, Ultrasound image enhancement: a review, Biomed. Signal Process Control. 7 (2012) 419–428, https://doi.org/10.1016/j.bspc.2012.02.002.

[7] C. a. Duarte-Salazar, andres E.A.E. Castro-Ospina, M. a. Becerra, E. Delgado-Trejos, Speckle noise reduction in ultrasound images for improving the metrological evaluation of biomedical applications: an overview, IEEE Access. 8 (2020) 15983–15999. <https://dx.doi.org/10.1109/aCCESS.2020.2967178>.

[8] S. V. Mohd Sagheer, S.N. George, A review on medical image denoising algorithms, Biomed. Signal Process. Control. 61 (2020) 102036. <https://dx.doi.org/10.1016/j.bspc.2020.102036>.

[9] A.F. Elnokrashy, Ultrasound speckle noise reduction based on motion compounding using optimized adaptive rood pattern search, in: Natl. Radio Sci. Conf. NRSC, Proc., IEEE, 2019, pp. 227–233, https://doi.org/10.1109/NRSC.2019.8734622.

[10] V.B. Shereena, G. Raju, Modified non-local means model for speckle noise reduction in ultrasound images, in: Lect. Notes Data Eng. Commun. Technol., Springer, 2022, pp. 691–707, https://doi.org/10.1007/978-981-16-9113-3_51.

[11] J.-S. Sen Lee, Digital image enhancement and noise filtering by use of local statistics, IEEE Trans. Pattern Anal. Mach. Intell. PAMI-2 (1980) 165–168, https://doi.org/10.1109/TPAMI.1980.4766994.

[12] D.T. Kuan, A.A. Sawchuk, T.C. Strand, P. Chavel, Adaptive noise smoothing filter for images with signal-dependent noise, IEEE Trans. Pattern Anal. Mach. Intell. PAMI-7 (1985) 165–177. <https://dx.doi.org/10.1109/TPAMI.1985.4767641>.

[13] V.S. Frost, J.A. Stiles, K.S. Shanmugan, J.C. Holtzman, A model for radar images and its application to adaptive digital filtering of multiplicative noise, IEEE Trans. Pattern Anal. Mach. Intell. PAMI-4 (1982) 157–166, https://doi.org/10.1109/TPAMI.1982.4767223.

[14] O. Magud, E.V.A. Tuba, N. Bacanin, Medical ultrasound image speckle noise reduction by adaptive median filter, WSEAS Trans. Biol. Biomed. 14 (2017) 38–46.

[15] J.I. Koo, S.B. Park, Speckle reduction with edge preservation in medical ultrasonic images using a homogeneous region growing mean filter (HRGMF), Ultrason, Imaging. 13 (1991) 211–237, https://doi.org/10.1177/016173469101300301.

[16] Tomasi, R. Manduchi, Bilateral filtering for gray and color images, in: Proc. IEEE Int. Conf. Comput. Vis., IEEE, 1998, pp. 839–846. <https://dx.doi.org/10.1109/iccv.1998.710815>.

[17] Y. Yu, S.T. Acton, Speckle reducing anisotropic diffusion, IEEE Trans. Image Process. 11 (2002) 1260–1270, https://doi.org/10.1109/TIP.2002.804276.

[18] Q. Guo, C. Zhang, Y. Zhang, H. Liu, An efficient SVD-based method for image denoising, IEEE Trans. Circuits Syst. Video Technol. 26 (2015) 868–880, https://doi.org/10.1109/TCSVT.2015.2416631.

[19] L. Shao, R. Yan, X. Li, Y. Liu, From heuristic optimization to dictionary learning: A review and comprehensive comparison of image denoising algorithms, IEEE Trans. Cybern. 44 (2014) 1001–1013, https://doi.org/10.1109/TCYB.2013.2278548.

[20] P.C. Tay, C.D. Garson, S.T. Acton, J.A. Hossack, Ultrasound despeckling for contrast enhancement, IEEE Trans. Image Process. 19 (2010) 1847–1860, https://doi.org/10.1109/TIP.2010.2044962.

[21] L. Zhu, C.W. Fu, M.S. Brown, P.A. Heng, A non-local low-rank framework for ultrasound speckle reduction, in: Proc. - 30th IEEE Conf. Comput. Vis. Pattern Recognition, CVPR 2017, 2017, pp. 493–501. <https://dx.doi.org/10.1109/CVPR.2017.60>.

[22] F. Mei, D. Zhang, Y. Yang, Improved non-local self-similarity measures for effective speckle noise reduction in ultrasound images, Comput. Methods Programs Biomed. 196 (2020), 105670, https://doi.org/10.1016/j.cmpb.2020.105670.

[23] G. Zhang, R. Song, B. Ding, Y. Zhu, H. Xue, J. Tu, J. Hang, X. Ye, D. Xu, Laplacian pyramid based nonlinear coherence diffusion for real-time ultrasound image speckle reduction, Appl. Acoust. 183 (2021), 108298, https://doi.org/10.1016/j.apacoust.2021.108298.

[24] M.E. Salih, X. Zhang, M. Ding, Kernel PCA based non-local means method for speckle reduction in medical ultrasound images, OALib. 09 (2022) 1–41, https://doi.org/10.4236/oalib.1108618.

[25] S. Pradeep, P. Nirmaladevi, A review on speckle noise reduction techniques in ultrasound medical images based on spatial domain, transform domain and CNN methods, IOP Conf. Ser. Mater. Sci. Eng. 1055 (2021), 012116, https://doi.org/10.1088/1757-899x/1055/1/012116.

[26] S. Shajun Nisha, S.P. Raja, Multiscale transform and shrinkage thresholding techniques for medical image denoising - performance evaluation, Cybern. Inf. Technol. 20 (2020) 130–146, https://doi.org/10.2478/cait-2020-0033.

[27] N. WangNo, S. Chiewchanwattana, K. Sunat, An efficient adaptive thresholding function optimized by a cuckoo search algorithm for a despeckling filter of medical ultrasound images, J. Ambient Intell. Humaniz. Comput. (2020) 1–26, https://doi.org/10.1007/s12652-020-01743-3.

[28] L. Jain, P. Singh, A novel wavelet thresholding rule for speckle reduction from ultrasound images, J. King Saud Univ. – Comput. Inf. Sci. 34 (2022) 4461–4471, https://doi.org/10.1016/j.jksuci.2020.10.009.

[29] S. Khare, P. Kaushik, Speckle filtering of ultrasonic images using weighted nuclear norm minimization in wavelet domain, Biomed. Signal Process. Control. 70 (2021), 102997, https://doi.org/10.1016/j.bspc.2021.102997.

[30] S. Cammarasana, P. Nicolardi, G. Patanè, Real-time denoising of ultrasound images based on deep learning, Med. Biol. Eng. Comput. 60 (2022) 2229–2244, https://doi.org/10.1007/s11517-022-02573-5.

[31] K. Zhang, W. Zuo, Y. Chen, D. Meng, L. Zhang, Beyond a gaussian denoiser: residual learning of deep cnn for image denoising, IEEE Trans. Image Process. 26 (2017) 3142–3155, https://doi.org/10.1109/TIP.2017.2662206.

[32] T. Koga, Motion compensated interframe coding for video-conferencing, in: Proc. Nat. Telecommun. Conf., 1981, pp. G5-3.

[33] K. Belloulata, S. Zhu, Z. Wang, A fast fractal video coding algorithm using cross-hexagon search for block motion estimation, ISRN Signal Process. 2011 (2011), https://doi.org/10.5402/2011/386128.

[34] S. Kamble, N. Thakur, P. Bajaj, Modified three-step search block matching motion estimation and weighted finite automata based fractal video compression, Int. J. Interact. Multimed. Artif. Intell. 4 (2017) 27, https://doi.org/10.9781/ijimai.2017.444.

[35] N. Rawat, M. Singh, B. Singh, Wavelet and total variation based method using adaptive regularization for speckle noise reduction in ultrasound images, Wirel. Pers. Commun. 106 (2019) 1547–1572, https://doi.org/10.1007/s11277-019-06229-w.

[36] S.L. Shabana Sulthana, M. Sucharitha, Kinetic Gas Molecule Optimization (KGMO)-based speckle noise reduction in ultrasound images, in: Soft Comput. Signal Process., Springer, 2022, pp. 447–455, https://doi.org/10.1007/978-981-16-1249-7_42.

[37] F. Memon, M. Ali Unar, M. Sheeraz, Image quality assessment for performance evaluation of focus measure operators, Mehran Univ. Res. J. Eng. Technol. 34 (2015) 389–386. <https://doi.org/10.48550/arXiv.1604.00546>.

[38] P. Kumar, S. Srivastava, Y. Padma Sai, S. Choudhary, Optimal Bayesian estimation framework for reduction of speckle noise from breast ultrasound images, in: Lect. Notes Electr. Eng., Springer, 2021, pp. 255–263, https://doi.org/10.1007/978-981-16-4149-7_22.

[39] H. Choi, J. Jeong, Despeckling images using a preprocessing filter and discrete wavelet transform-based noise reduction techniques, IEEE Sens. J. 18 (2018). 3131–3139.https://dx.doi.org/10.1109/JSEN.2018.2794550.
[40] K. Murugesan, P. Balasubramani, P.R. Murugan, A quantitative assessment of speckle noise reduction in SAR images using TLFFBP neural network, Arab. J. Geosci. 13 (2020) 1–17, https://doi.org/10.1007/s12517-019-4900-4.
[41] A. Jφ, N.B.S. Jensen, Calculation of pressure fields from arbitrarily shaped, apodized, and excited ultrasound transducers, IEEE Trans. Ultrason. Ferroelectr. Freq. Control. 39 (1992) 262–267, https://doi.org/10.1109/58.139123.
[42] R. Rosa, F.C. Monteiro, Performance analysis of speckle ultrasound image filtering, Comput. Methods Biomech. Biomed. Eng. Imaging Vis. 4 (2016) 193–201, https://doi.org/10.1080/21681163.2014.935803.
[43] O. Rubel, V. Lukin, A. Rubel, K. Egiazarian, Selection of lee filter window size based on despeckling efficiency prediction for sentinel sar images, Remote Sens. 13 (2021). 1887.https://dx.doi.org/10.3390/rs13101887.
[44] H. Choi, J. Jeong, Speckle noise reduction for ultrasound images by using speckle reducing anisotropic diffusion and Bayes threshold, J. Xray. Sci. Technol. 27 (2019) 885–898, https://doi.org/10.3233/XST-190515.